Reinforcing a Direct Bond between Optical Materials by Filamentation Based Femtosecond Laser Welding

David Hélie[*], Fabrice Lacroix[**] and Réal Vallée[*]

[*] *Center for Optics, Photonics and Lasers, Université Laval, 2375 rue de la Terrasse, Québec, Qc, G1V 0A6, Canada.*
E-mail: david.helie.1@ulaval.ca
[**] *Institut Franco-allemand de Recherches de Saint-Louis, 5 rue du General Cassagnou, 68300, Saint-Louis, France.*

We propose a joining process using femtosecond laser micro-welding to reinforce a direct bond. The process, which is executed at ambient temperature and can be applied to both similar and dissimilar material combinations, consists in inscribing weld lines in a closed loop forming a sealing pattern at the outskirts of the direct bond, thus preventing it from lifting off. We first characterized the size of material modification following exposure to focused femtosecond laser pulses at the direct bonded interface and its dependence on processing parameters. The derived optimal joining conditions are then applied to join fused silica-fused silica and fused silica-BK7 assemblies. Statistical measurements show an approximate threefold reinforcement factor after writing 11 weld lines in a rectangular pattern with rounded corners. This data was fitted with the two-parameter-Weibull-model which gives insight on the performance and reliability of the process.
DOI:10.2961/jlmn.2012.03.0010
Keywords: Direct Bond, Bonding, Joining, Laser welding, Femtosecond laser, Filamentation, Nonlinear Kerr effect, Ultrashort laser pulses, Glass.

1. Introduction

Optical materials, such as glasses and semi-conductors, are increasingly popular in the fields of optics, electronics, telecommunications, biology and medicine. Transparent material joining techniques are constantly evolving to adapt to the specific constraints and standards of these industries. Many glass-based applications require optimal optical transmission properties as well as the absence of bonding agents, such as adhesives and other organic chemicals, since they are a source of premature aging and degassing. The miniaturization of components greatly discourages the use of mechanical mounts as an alternative to adhesives. Luckily, several adhesive-less joining processes have been developed, such as anodic bonding, solid-state diffusion bonding, CO_2 laser fusing and thermal annealing of optical contact (i.e. direct bond) [1-6]. Bonds made with most of these techniques are almost as strong as the base materials. However, they either induce or require macroscopic heating of the components and therefore material combinations are restricted by the mismatch of thermal expansion properties.

One alternative to heating and gluing glass components is to use welding by means of ultra-short laser pulses [7]. As opposed to far-infrared cw lasers used to fuse glass, visible and near-infrared ultra-short laser pulses can be focused completely inside the glass block, without affecting its surface. The high peak intensity at the focus sets proper conditions for non-linear absorption of energy through multi-photon, tunneling and avalanche processes [8,9]. When such phenomena occur at an optically contacted interface between two transparent materials, ionization will result in local melting and welding of the two components. No additional material or specific surface treatment is necessary to induce local absorption of laser energy. However, the gap between materials must be smaller than $\lambda/4$ otherwise laser exposure will ablate the surfaces and not result in joining [10]. Microscopic weld seams are written by scanning the focused laser along the interface between the two materials. Compared to other glass joining techniques, this process is executed in ambient conditions and material modification is confined to the vicinity of the focus. Therefore, the absence of macroscopic heating makes this a suitable process for joining materials with a great mismatch in their thermal dilatation properties as long one of them is transparent to the ultra-short laser pulses.

In this work, we present an application of femtosecond laser welding: the sealing and mechanical reinforcement of a direct bond between similar and dissimilar optical materials. Firstly, the influence of laser processing parameters on the size of material modification is analyzed at the interface between fused silica and fused silica – BK7 assemblies. This study paved the way to choosing optimal processing parameters for conducting a statistical analysis of the shear joint strength of direct bonds between fused silica substrates sealed by femtosecond laser welding. Results show an approximate threefold increase in joint strength of direct bonds by welding only a small part of the total direct bonded area. We also discuss the performance and reliability of this application by fitting our shear strength measurements to the two parameter Weibull model.

2. Joining Glass with Ultra-short Laser Pulses

2.1 Heat Accumulation vs. Filamentation

Previous works on welding of glass with ultra-short laser pulses followed two main trends. Some use MHz repetition rate systems emitting pulses with a duration of a few hundred femtoseconds (fs) to several picoseconds (ps) [11-17]. The time between successive pulses is much shorter than the time necessary for the material to diffuse thermal energy out of the focal volume. Exposure to a great number of focused laser pulses will generate important heat accumulation at the interface between glass based materials thereby creating a melting pool from which the materials fuse together. With optimized processing parameters, the bond strength of weld seams is reported to be almost as high as the base materials [16,17]. Although focusing lenses with high numerical apertures are needed, the use of this technique can weld glass at high scan speeds.

Another approach consists in harnessing non-linear propagation effects such as self-focusing and filamentation instead of heat accumulation [7,10,18-22]. Evidence of heat accumulation is generally not observed at repetition rates below 200 kHz. Pulses emitted from chirped pulse amplification systems at kHz repetition rates with sub-100 fs durations can easily reach the peak power needed to create optical filaments up to several hundred μm in length [23,24]. When such an intense ultra-short laser pulse propagates in n_2 positive material, the peak of the pulse will see a slightly higher index of refraction than the wings. This uneven refractive index profile acts as a focusing lens, where the peak of the pulse will self-focus the strongest and collapse first along the propagation. When using external focusing, the peak of the pulse will collapse before the optical system's geometrical focus. This point of collapse marks the beginning of the filament and other parts of the pulse will collapse further along the propagation until diffraction over comes self-focusing. The filament length is primarily controlled by the pulse energy. When these filaments cross an optically contacted interface between two transparent materials, the ionization and plasma relaxation inside the filament will transfer the absorbed laser energy to the material. The pressure build-up inside the focal volume will induce microscopic surface deformations which are responsible for mixing of the molten material inside the filament zone [19,20]. Very fast cooling of the exposed region results in a weld seam whose width is confined to a few μm. Although the scan speed is slower than for heat accumulation, the absence of important heat affected zones makes it possible to weld dissimilar materials with a great mismatch between thermal dilatation properties, for example such as glass and metal [19,22]. Furthermore, transmission welding by filamentation of fs pulses is possible for materials with a thickness of several mm since the focusing lens typically has a working distance beyond 10 mm. Both welding by heat accumulation and filamentation have their distinct benefits and have shown great potential for manufacturing and assembly of miniature components.

2.2 Optical Contacting as a pre-joining method

The first demonstrations of welding with ultra-short pulses were executed with the use of a clamping device to induce a small region of optical contact between materials prior to welding [7,10,21]. Results showed a joint strength of several MPa but clamping of the materials induced important mechanical constraints afterward around the welded region and degraded the joint strength. Recent reports propose the use of optical contacting, or direct bonding, as a prejoining method prior to welding [11-13,15-19]. Materials with sufficient surface quality can be physically bound by Van der Waals forces acting over an important part of the area between the bonding surfaces [3-5]. The joint strength of weld seams written by ultra-short laser pulses can reach up to 95% of the strength of the pristine bulk material in such conditions with optimized processing parameters [16]. However, some attempts at measuring the joint strength of weld seams between thick plates also included the contributions of optical contact. Important uncertainties arise from efforts to subtract the strength of optical contact to the total strength of assemblies to isolate the sole strength of weld seams [12,13]. Furthermore, the lift-off of optical contact at the edges of the assemblies and the refractive index change through the weld seams alter the component's optical transmission properties.

2.3 Reinforcing a Direct Bond with Femtosecond Laser Pulses

In an effort to circumvent previously underlined flaws, we recently proposed to use welding by filamentation of femtosecond laser pulses to seal the outskirts of a direct bonded region [18,19]. Direct bonding implies the use of materials with appropriate surface roughness and flatness to achieve a state of optical contact preferably over the whole area between bonding surfaces [5]. Sealing the inner part of the direct bond using either a rectangular or circular pattern prevents lift-off typically initiated by impact loads and thermal shocks. Furthermore, the assembly's optical transmission properties are not altered inside the sealed area. Reinforced assemblies show greater resistance to mechanical and thermal constraints than those that are unreinforced [18]. Furthermore, this joining process is executed in ambient conditions such that it is most suitable to join dissimilar materials with important mismatch in their thermal properties as long as one of them is transparent to the laser's wavelength. The combination of direct bonding with an adequate laser exposure strategy can benefit from both underlining processes, as we show hereafter.

3. Experiments

3.1 Materials

All experiments were performed with UV grade fused silica and BK7 substrates. For fused silica only assemblies, rectangular 10 x 15 mm^2 windows of 2 millimeter thickness were direct bonded to 15 x 20 mm^2. For fused silica – BK7 assemblies, factory polished BK7 samples of a 1 mm thickness and 13 mm diameter were direct bonded to 15 x 20 mm^2 fused silica windows. Both materials have a 60-40 scratch dig surface quality. Flatness was evaluated to be better than $\lambda/4$ for fused silica and better than λ for BK7 according to the suppliers.

3.2 Cleanliness and Bond Quality

Careful consideration is required to obtain direct bonding. Apart from the surface quality and flatness, substrates must not show scratches or similar damage features at their bonding surfaces. Prior to direct bonding, the substrates

must be thoroughly cleaned to eliminate all physical and chemical contaminants at the surfaces. Subsequently, direct bonding is achieved by simply stacking the two samples which produces an interference pattern at the bonding surfaces. Then, applying a light pressure at the center will establish a first point of optical contact which will quickly extend to cover the whole area between the bonding surfaces. Following this step, it may sometimes be necessary to apply pressure at specific point to extend the optical contact to the whole area and avoid its further lift-off. However so, the inability to achieve a state of optical contact over the whole area even after applying pressure at specific regions is most certainly due to either surface damage, unsuitable cleanliness and/or insufficient flatness. In these cases, the assemblies were discarded from our experiments.

3.3 Experimental setup

The setup used for laser welding is illustrated in Fig. 1. We used a Coherent REGA 9050 Titanium-sapphire femtosecond laser system based on chirped pulse amplification. Laser parameters are listed in table 1. The average power delivered to the sample is controlled by adjusting the waveplate's axis with respect to that of the polarizer. In all welding experiments, the polarizer's axis is oriented in the *x* direction and focusing of the pulses is ensured by a 10X 0.16 NA microscope objective lens. The samples are installed in a custom holder which is mounted on top of a 3 axis motorized translation stage system (Newport XPS) with goniometers for alignment. Using a custom interface with this scanning apparatus, the user can perform basic linear scans as well as programmed rectangular and circular contours in the *xy* plane.

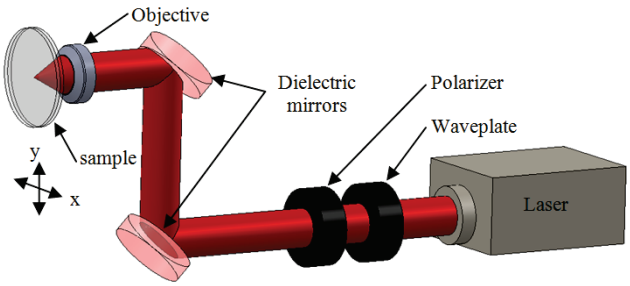

Fig. 1 Illustration of the setup used for laser welding.

Table 1 Laser parameters of the REGA 9050 laser system

Parameter	Value
Repetition rate	10 - 300 kHz
Central wavelength	787 nm
Minimum pulse width (FWHM)	70 fs
Maximum average power	1.25 W
Maximum pulse energy	5 µJ @ 250 kHz
Polarization	Linear in *x* direction

4. Results

4.1 The Influence of Pulse Energy and Focus Depth on Filament Length

In the context of femtosecond laser welding of glass based on heat accumulation, several groups have shown how the processing parameters influence the size of the molten pool [16-18]. Alternatively, in the case of femtosecond laser glass welding based on non-linear filamentation effect, Kongsuwan and al. have analyzed the feature size and weld seam morphology in BK7 with a 1 kHz femtosecond laser system [20]. In this section, we present a similar study between fused silica-fused silica and fused silica – BK7 assemblies using a 250 kHz repetition rate. The use of 250 kHz pulse train allows to increase the scan speed by two orders of magnitude (with respect to 1 kHz) and still obtain an equivalent spatial overlap of pulses during scanning.

The goal of the following procedure was to observe optical filaments crossing the interface at different depths and evaluate the extent of material modification at the interface. After direct bonding of the substrates, multiple scanning of the focused laser pulse in the bulk was performed at a fixed repetition rate and scan speed while varying the pulse energy and the position of the focus. Scan lines were oriented along the *x* direction and equally spaced at steps of 20 µm in the *y* direction. Inscription of each set of scan lines was performed by setting a constant pulse energy and varying the focus position at steps of 20 µm in the *z* direction between each scan line. The whole process was repeated for pulse energies of 0.2 to 1.1 µJ with increments of 0.1 µJ. Table 2 shows the scan parameters involved in this experiment. Following laser exposure, the substrates were cut perpendicularly to the scan lines. The slices of the cuts were then grinded and polished with a 0.3 µm cerium oxide slurry. This gave us a clean cross-section view of the scan lines for viewing with a scanning electron microscope (SEM). Figure 2a shows a typical SEM image of 3 scan lines written with 0.6 µJ pulses near the direct bonded interface of two fused silica windows.

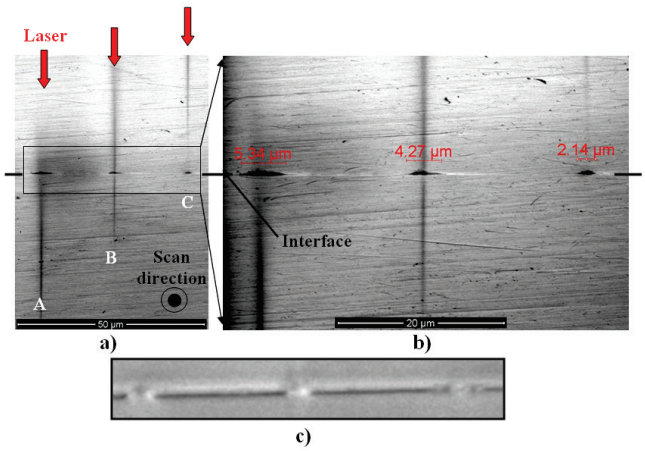

Fig. 2 a) SEM image of the cross section of optical filament tracks written with 0.6 µJ pulses near the direct bonded interface between two fused silica windows. Scan lines A, B and C were inscribed at different focus positions with pulses incident from the top. **b)** Close-up view with SEM of the interaction of optical filaments with the interface. **c)** optical microscope image showing a local continuity of the material where the interaction of the filaments took place. (Laser: 0.6 µJ, 787 nm, 70 fs, 250 kHz, 1 mm/s)

Lines A, B and C were written at focus locations of 1620 µm, 1600 µm and 1580 µm respectively. Focus location was evaluated with respect to a reference position at the front surface of the sample where focused pulses in air induce plasma with white light generation visible to the naked eye. Once this reference position is found, the sample is moved towards the focusing objective according to the amount specified by the focus location. For this particu-

lar experiment, fused silica substrates of 2.3 mm thickness were used. The measured focus locations are consistent with the optical thickness of the material equal to *n* x *focus depth*.

Table 2 Experimental conditions used for the multiple scanning experiment

Parameter	Value
Average power	50 - 275 mW
Pulse energy	0.2 – 1.1 μJ
Repetition rate	250 kHz
Central wavelength	787 nm
Minimum pulse width (FWHM)	70 fs
Polarization	// to scan direction
Focusing objective	10X 0.16 NA
Effective focal length	15.4 mm
Clear aperture	5 mm

Exposure of fused silica in these conditions results in a smooth refractive index change of width smaller than 2 μm along the filament zone. The length of the material modification extends beyond the Raleigh range $2z_0$ (≈ 28μm) which is consistent with reports on filamentation of fs pulses in condensed matter [23,24]. The close-up view of the parts of the filaments that cross the interface (figure 2b) reveals that the width of interaction is somewhat larger than the trace of refractive index change and depends on focusing conditions and pulse energy. Figure 2c shows this same set of scan lines viewed through an optical microscope. Interactions with the interface show a local continuity of the material in a manner analogue to welding. Further details of the filaments' interaction with the interface will be treated in subsection 4.2.

Figure 3 shows cross section views of the material modifications across the direct bonded interface (focus location of 1600 μm) between fused silica and BK7 induced at different pulse energies. As opposed to fused silica, BK7 glass indicates evidence of heat accumulation after exposure to pulses having energies beyond 0.3 μJ. The heat affected zone (HAZ) in BK7 is abruptly halted at the interface by a clear cut difference in heat accumulation effects compared with fused silica. The material modification in fused silica continues as a relatively smooth line of refractive index change induced by filamentation with no HAZ. Nevertheless, the interaction of filaments at the interface in these conditions shows similar behavior to that of two direct bonded fused silica windows. Both the length and the width of material modification expand with increasing pulse energies.

Fig 4 presents measurements of the length of modified regions induced by filamentation as function of the pulse energy at three different focus locations in both fused silica and fused silica-BK7 assemblies. Focus positions were chosen so as to induce filaments before (1560 μm) and beyond (1640 μm) the interface, as well as when filaments are centered thereupon (1600 μm). The global uncertainty of each measurement is evaluated to be approximately 2 μm. In all cases, the filament length is proportional to the pulse energy as expected. However, results suggest that the length of modified regions is slightly lower after passing the interface between two direct bonded fused silica

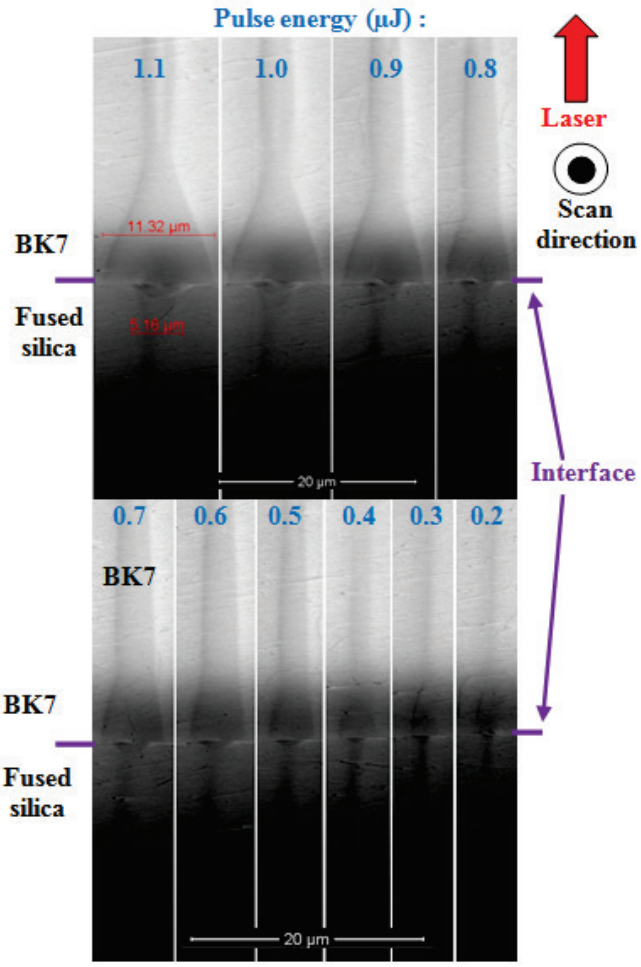

Fig. 3 SEM images of the cross section of optical filaments written at different pulse energies near the direct bonded interface between fused silica (bottom) and BK7 (top). (Laser: 0.2 – 1.1 μJ, 787 nm, 70 fs, 250 kHz, 1 mm/s)

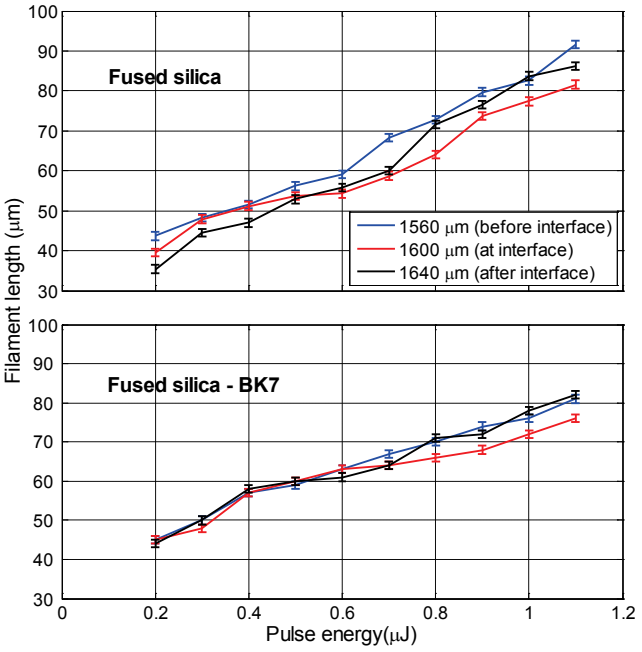

Fig. 4 Measurements of filament length as function of incident pulse energy at three different focus locations for fused silica (top) and fused silica – BK7 (bottom) components. (Laser: 0.2 – 1.1 μJ, 787 nm, 70 fs, 250 kHz, 1 mm/s)

windows. We suspect this decrease in length is due to the altered dynamics of self-focusing when the pulses pass the interface. The case of fused silica – BK7 shows very similar behavior when filaments are centered upon the interface. Otherwise, the material modification length measurements before and after the interface are very alike. The decrease of filament length after passing the direct bonded interface may be counterbalanced by a HAZ slightly longer than the filament length in BK7.

4.2 Width of Interaction at the Interface

Figures 2b and 3 show that the width of interaction at the interface depends on both the pulse energy and the focus location. Kongsuwan et al. have reported that increasing the pulse energy will result in larger weld seam widths when using filamentation of fs pulses to join BK7 glass [20]. We sought out to investigate this trend for our particular processing parameters firstly by peeling off the joint surfaces so as to observe and measure the width of the damage tracks due to breakage of weld lines. As can be seen in figure 5a, the material around the weld seams breaks in a brittle and unpredictable manner. Although the extent of damage is reduced following exposure to lower pulse energies (figure 5b), big chunks of material with a width larger than that of the set of scan lines are removed when welding at high pulse energies (figure 5c). Measurements of the width of damage tracks after peeling off the samples yield great uncertainty. We did notice that at low pulse energies, the mean widths of the damage tracks are comparable to the width of interaction at the interface when viewing the cross section before peeling off the samples (figures 2 and 3). Therefore, we determined that the width of interaction at the interface can be properly approximated through the observation of cross sections. Figure 6 presents measurements of the width of interaction at the interface as a function of pulse energy for four different focus locations in a fused silica assembly. The measurement uncertainty is evaluated to be approximately 0.2 µm. The inset of Fig 6 shows the relative position (colored line) where the interface is positioned with respect to the filaments.

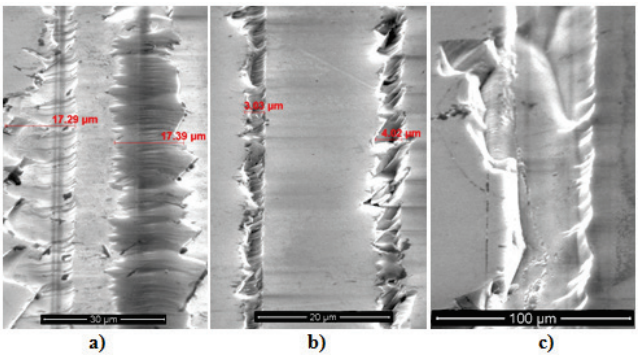

Fig. 5 SEM images of the damage tracks at the peeled off surface of fused silica induced by weld lines written at pulse energies of **a)** 0.8 µJ, **b)** 0.4 µJ and **c)** 1.1 µJ. (Laser: 787 nm, 70 fs, 250 kHz, 1 mm/s)

According to the slice by slice self-focusing model proposed by Chin and al., the laser pulse can be separated into temporal slices each yielding a different peak intensity [24]. They will self-focus and collapse at different positions along the propagation. The peak of the pulse, carrying the highest intensity, will undergo the strongest self-focusing and collapse closest to the focusing objective. The slices carrying energy from the sides of the pulse will not self-focus as strongly and collapse near the end of the filament. Regarding to the inset of figure 6, focus positions 1 and 2 imply that the end part of the filament crosses the interface. Increasing the pulse energy will slightly intensify the slices collapsing in these regions. As a result, measurements of figure 6 for focus positions 1 and 2 show a slow and steady rise of the width of interaction as a function of pulse energy. When the part of the filament at focus position 3 crosses the interface, the most intense slices of the pulse collapse near the interface thereby resulting in a more rapid growth of the width of interaction with respect to the pulse energy. As the filaments lengthen with increasing pulse energy, an interaction is observed beyond pulse energies of 0.6 µJ at position 4.

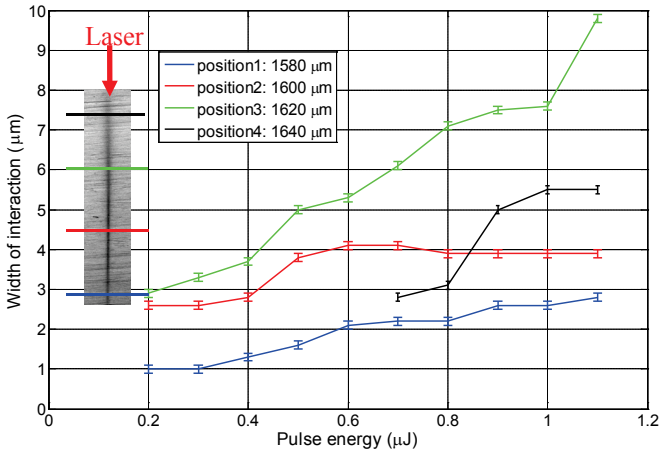

Fig. 6 Measurements of the weld seam width at the direct bonded interface between fused silica windows as function of incident pulse energy at four different focus locations in fused silica. The inset shows where the weld seam is formed along the filament for each focus depth. (Laser: 0.2 – 1.1 µJ, 787 nm, 70 fs, 250 kHz, 1 mm/s)

We repeated the above measurements for weld lines written in a fused silica – BK7 assembly. We also measured the width of the HAZ in BK7 where it is abruptly cut off at the interface, as shown in figure 3. Figure 7 presents measurements of the width of these interactions for the two focus locations where an interaction at the interface was observed. The measured width of interaction at position 1 (blue curve) follows the same trend as the results presented in figure 6 for the same focus position. At this focus position, the less intense slices of the pulse are self-focused near the interface and into BK7, thereby gradually increasing the width of interaction and HAZ in BK7 (black curve). When the focus location is at position 2, the most intense slices of the pulse are self-focused near the interface and into BK7, thereby further increasing the width of interaction at the interface (red curve). The width of the HAZ in BK7 (fuchsia curve) is generally twice as large as the width of interaction. Although figure 3 suggests that successful welding has occurred, the mismatch between thermal expansion properties may induce important stress to the bonded region with rising heat accumulation effects in BK7. We have observed for some samples that the induced stress

is strong enough to break the optical contact around the welded region. Therefore, it is preferable to adjust the pulse energy accordingly and thereby avoid inducing important HAZ and unwanted effects.

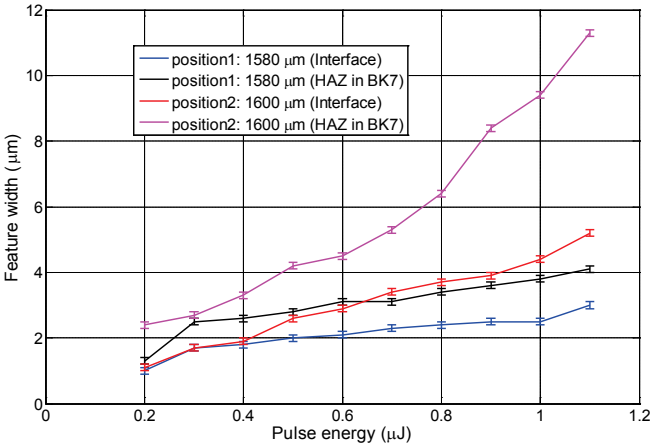

Fig. 7 Measurements of the width of interaction at the interface and the width of the heat affected zone (HAZ) in BK7 at two different focus locations as function of incident pulse energy near the direct bonded interface between fused silica and BK7. (Laser: 0.2 – 1.1 μJ, 787 nm, 70 fs, 250 kHz, 1 mm/s)

The results presented in this section clearly demonstrate that the processing parameters influence the length of material modification and the width of interaction at the direct bonded interface between two transparent materials. Local welding with a precision of a few μm is observed as long as a part of the optical filaments crosses the direct bonded interface. As was expressed in reference [25], one can benefit from the elongated form of the filaments and increase the pulse energy to lower the setup's positioning and alignment accuracy. On the other hand, this strategy will increase the extent of material modification around the weld seam which most certainly influences the joint strength of the material around the weld seam. This was shown in figure 5 where chunks of material larger than the width of the filaments were damaged after peeling off welded samples. Likewise, these observations may also imply that the joint strength of the welded region can approach that of the base material, as was demonstrated when welding with fs laser pulses at high repetition rates [16,17]. A complimentary study to our work would be to evaluate the weld seam strength for each of the laser exposure conditions that were considered. However, since the direct bond contributes to the total strength of the assemblies, no mechanical testing strategy can isolate the strength of single weld lines with acceptable precision. The approach proposed by Roth et al. of inserting a knife blade between the glass pieces to measure the bond energy is unfortunately not suitable for thick samples such as the ones we used [11]. We rather adopted shear strength testing presented through Weibull analysis since this tool offers an excellent statistical viewpoint for the interpretation of results.

4.3 Shear stress measurements

Specific details of the shear strength testing conditions and setup are presented in reference [18]. We chose one exposure condition amongst those discussed in subsections 4.1 and 4.2 and conducted a statistical evaluation of the joint strength of direct bonds between fused silica windows with and without fs laser weld lines. For this experiment, 10x15 mm^2 fused silica windows of 2 mm thickness were direct bonded to 15x20 mm^2 of the same material so as to obtain 44 samples joined over an area of 9.6x14.6 mm^2 (the windows have chamfered edges). Eleven weld lines with 10 μm spacing were inscribed in half of these samples following a rectangular geometry in order to seal an 8x12 mm^2 region with rounded corners of 2 mm radius. Laser parameters were set to 250 kHz, 70 fs, 790 nm, 0.5 μJ, 1 mm/s and focus location at position 3. According to figure 5, the weld seam width is approximated to be 5 μm, such that the total area corresponding to weld seams is 2.2 mm^2. Shear stress was calculated over the whole direct bonded area, which is equal to 140 mm^2, after measuring the applied shear load at breakage of each sample. The settling time between direct bonding and shear stress measurements was between 24 to 48 hours. Figure 8 shows a Weibull plot of the shear stress measurements at breakage of direct bonded samples with and without weld lines.

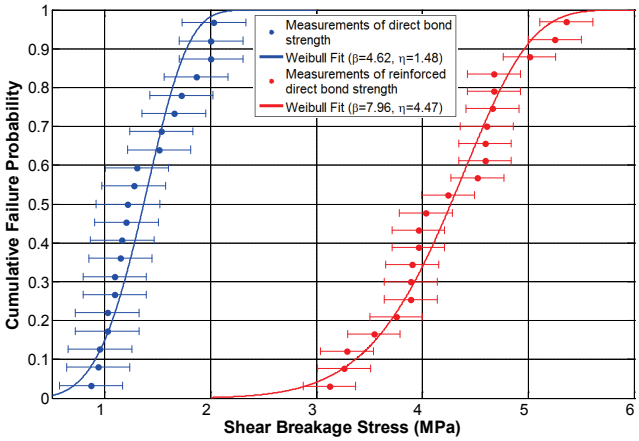

Fig. 8 Weibull plot of shear strength measurements at breakage of direct bonds with and without laser reinforcement. (Laser: 0.5 μJ, 787 nm, 70 fs, 250 kHz, 1 mm/s)

In this plot, each point represents a measurement of the applied shear stress (abscissa) at breakage of each sample. For each group of measurements (with and without reinforcement), the data was classified in increasing order so as to calculate the cumulative failure probability (ordinate) from Bernard's approximation of the median rank [26]. This approximation's accuracy is higher than 99% and is more convenient than the interpolation method to obtain the median ranks. The error bars take into account several experimental details which are difficult to control, including the variable quality of optical contact as well as the fact that the mount used for shear load testing could not guarantee that only shear stress was applied. We suspect that small but non-negligible tensile stress and torsion was applied during measurements. The curves fitted to the measurements were obtained according to the two parameter Weibull model of equation (1).

$$F(x) = 1 - e^{\left(\frac{-x}{\eta}\right)^{\beta}} \quad (1)$$

The β shape and η scale parameters are calculated for each set of measurements using the least squares method

and are specified in the legend of the plot [26]. Results clearly indicate that samples with eleven weld lines were reinforced. An approximate threefold increase in resistance to shear strength is observed. The detailed Weibull analysis is presented hereafter at subsection 4.4.

The measured strengths of optical contact without laser reinforcement in our experiment are higher than those reported in other work on welding with ultrashort pulses [12,13]. Although the strength of the bond can vary according to the materials and surface preparation, we observed that samples showing regions of lift-off of optical contact around the direct bonded region, similar to those used in references 12 and 13, do not resist well to applied stress. This lift-off acts in a manner analogous to a crack or other defect in a material thereby reducing the bond's resistance. Samples for which optical contact was achieved over the whole area are much harder to separate since the absence of lift-off does not initiate the breakage of the bond. However, once this lift-off is initiated by continuously applied stress, the bond will break in a very fast and fragile manner. Therefore, our measurements account for the threshold of lift-off of optical contact. When weld lines are inscribed at the edges of the direct bonded region, qualitative observation of samples show that this lift-off is halted at the weld seam such that the central sealed area is better protected against the lift-off of optical contact [11]. The breakage stress measurements of figure 8 for reinforced samples suggest that once the threshold for lift-off of optical contact is reached, increasing the load will build-up stress at the periphery of the sealed area until the fracture strength of the weld seam is reached thereby breaking the bond.

Since only a very small portion of the direct bonded area was welded and by the sealed region's ability to resist to lift-off of optical contact, results confirm that the intrinsic strength of weld seams induced by the filamentation effect can withstand greater stress than direct bonded regions. This idea is supported by the formation of strong covalent bonds inside the welded region whose strength is mainly dictated by the nature of atoms and molecules forming the bond [11]. In the absence of mechanical stress, the joint strength of welded regions written with ultrashort laser pulses can approach that of the pristine bulk material. On the other hand, Van der Waals bonds can form between any pair of atoms and molecules but have a bond energy typically one to two orders of magnitude weaker than that of covalent bonds [4,11]. Furthermore, the Van der Waals bond energy depends on the distance between particles which can vary over the whole direct bonded area [6]. These factors may account for the variability of the measurements and thus support the presentation and interpretation of such data following Weibull analysis [26].

4.4 Weibull Analysis

The Weibull parameters derived from the measurements of figure 8 are shown in table 3. Mean and median values confirm an approximate threefold increase in shear strength. The Weibull parameters β and η used to calculate the fit for each set of measurements are also specified in table 3. The correlation coefficients r show a good fit between the experimental data and the two parameter Weibull model. The shape parameter β determines the slope of the fit and gives information about the reliability of the studied processes and testing methods. In the present scope of failure analysis, a slope of $\beta < 1$ will spread out the data in the plot and suggests that either the testing method and/or assembling of components may be inappropriate. The use of samples with inadequate quality, for example with surface or in the bulk defects, may also imply that two or more failure modes were measured in the data. Therefore, a pretest may be necessary to filter out bad components for the study. In our experiment, this was done by eliminating the direct bonded assemblies showing lift-off of optical contact. Distributions with slope fits of $\beta > 1$ are typically sought-after, which is the case of both sets of measurements in figure 8. In these circumstances, the reliability of the components can be approximated much better so as to define the proper operating conditions. For example, the *B10* life can serve as a parameter to determine the maximum operating conditions of the component. The *B10* life is evaluated from the fit by taking the value of stress for which the cumulative failure probability is equal to 0.1 (i.e. 10% of components will fail). In manufacturing, it may be quite advantageous and more cost effective to use this criterion as a reference and filter out the 10% of components with inadequate strength. However, one drawback of obtaining distributions with $\beta > 4$ is that exceeding the operating conditions is costly and will most certainly result in failure of most of the components.

Mathematically, the scale parameter η represents the abscissa value of the fit for an ordinate of 63.2%. It is most useful in Weibull theory, along with β, to calculate the mean stress at failure (MSAF) with the help of equation 2. The MSAF parameter is used to evaluate the stress for which approximately 50% of components will fail. Values of the MSAF are shown in table 3 and are within 5% of the geometrical mean values of each set of measurements. We expect that the MSAF will increase if more weld lines are used to seal a direct bonded region.

Table 3 Weibull parameters for each set of measurements

Parameter	Direct Bond	Reinforced Direct Bond
Mean (*MPa*)	1.31	3.98
Median (*MPa*)	1.22	4.24
Standard deviation (*MPa*)	0.38	0.97
r [1]	0.938	0.977
β [2]	4.62	7.96
B10 (*MPa*) [3]	0.91	3.37
η (*MPa*) [4]	1.48	4.47
MSAF (*MPa*) [5]	1.35	4.21

[1] Correlation coefficient
[2] Weibull slope or shape parameter
[3] "B" Life: Value of x for $F(x) = 10\%$
[4] Characteristic life or scale parameter
[5] Mean Stress At Failure (equivalent to Mean Time To Failure from [26])

$$MSAF(\beta,\eta) = \eta\Gamma\left(1+\frac{1}{\beta}\right) \quad (2)$$

The shear strength measurements presented in figure 8 show an acceptable fit to the Weibull two parameter model and the reliability of components assembled by laser reinforced direct bonding was discussed accordingly. Since the experimental data correlates well to the Weibull model whose β shape parameter is high, it can serve to establish

reliable predictions of safe operating conditions for components assembled according to our process. For example, a direct bonded component must be designed to resist to maximum shear loads of 40 Kg, which is equivalent to an applied stress of 2.8 MPa. The Weibull fits predict that 99% of direct bonds will break. This proportion becomes less than 5% after laser reinforcement by 11 weld lines and can be further diminished by increasing the number of weld lines around the sealed area. The flexible geometry and processing parameters offered by the laser reinforcement strategy presented in this work can be adjusted according to the needed requirements of direct bonded assemblies.

5. Conclusion

In this work, we have measured the extent of the interaction of focused fs laser pulses at the direct bonded interface during micro-welding of glass. We have also demonstrated its application to the reinforcement of a direct bond. By sealing a direct bonded region by fs laser welding, we are able to reliably join transparent materials without affecting their optical transmission properties. Firstly, we studied the influence of processing parameters, notably the pulse energy and focus location, between similar (fused silica) and dissimilar transparent material combinations (fused silica – BK7). Results show that the length of optical filaments may be slightly diminished after passing the direct bonded interface. Furthermore, the width of interaction at the interface depends on both the pulse energy and the focus location. This is in good agreement with past work using filamentation of fs laser pulses to weld glass [20]. This analysis of the material modification at the interface between fused silica and BK7 showed that micro-welding is feasible even when only one material shows evidence of heat accumulation. A great miniaturization potential was demonstrated since the measured widths of interaction for one pass with the laser with the specified processing parameters are below 10 μm.

We applied the fs laser micro-welding process to mechanically reinforce a direct bonded region between fused silica glass components. Compared to other methods for reinforcing a direct bond where macroscopic heating is necessary, the one presented in this work is applicable to transparent and transparent-opaque materials combinations disregarding the mismatch of thermal properties between dissimilar materials. Furthermore, sealing the direct bonded regions between dissimilar materials increases the components resistance to both mechanical loads and thermal shocks [18]. Our measurements of the shear strength at breakage of components statistically demonstrate an approximate threefold reinforcement factor after the inscription of eleven rectangular shaped weld lines with rounded corners. Our measurements were fitted with the Weibull two parameter model which served to evaluate the performance and establish basic guidelines for defining the reliability of our process. By combining direct bonding and fs laser micro-welding, this joining process would be of great aid in manufacturing of robust high precision optical components, assembling of high power emission devices, aerospace engineering and many other applications where operating conditions are not conducive to the use of organic agents and adhesives.

Acknowledgements

We are truly grateful for the help of Daniel Gingras and Stéphan Gagnon for SEM measurements. Special thanks to the engineering team at Doric Lenses Inc for polishing and sample preparation. Financial support from the FQRNT (Fonds de recherche du Québec – Nature et technologies), the NSERC (National Science and Engineering Research Council of Canada) and the CIPI (Canadian Institute for Photonic Innovation) is acknowledged.

References

[1] D. I. Pomerantz: U.S. Patent 3397278 (1968).
[2] J. Haisma, C. L. Alting and T. M. Michielson: U.S. Patent 5009689 (1991).
[3] J. Haisma and G.A.C.M. Spierings: Mat. Sc. Eng., 37, (2002) 1.
[4] J. Haisma, N. Hattu, J. T. C. M. Pulles, E. Steding and J. C. G. Vervest : App. Opt., 46, (2007) 6793.
[5] J. Haisma, G.A.C.M. Spierings, T. M. Michielson and C. L. Adema: Philips J. Res., 49, (1995) 23.
[6] V Greco, F Marchesini and G Molesini: J. Opt. A Pure Appl. Opt., 3, (2001) 85.
[7] T. Tamaki, W. Watanabe, J. Nishii and K. Itoh: Jap. Jour. App. Phys., 44, (2005) L687.
[8] C. B. Schaffer, A. Brodeur and E. Mazur: Meas. Sci. Technol., 12, (2001) 1784.
[9] R.R. Gattass and E. Mazur: Nat. Phot., 2, (2008) 219.
[10] W. Watanabe, S. Onda, T. Tamaki, K. Itoh and J. Nishii: App. Phys. Let., 89, (2006) 021106.
[11] S. Roth, K. Cvecek, I. Miyamoto and M. Schmidt: Proc. SPIE, 7920, (2011) 792006.
[12] K. Cvecek, I. Miyamoto, J. Strauss, M. Wolf, T. Frick and M. Schmidt: App. Opt., 50, (2011) 1941.
[13] K. Cvecek, I. Miyamoto, J. Strauss, V. Bui, S. Scharfenberg, T. Frick and M. Schmidt: JLMN-Jour. Laser Micro/Nanoeng., 7, (2012) 68.
[14] A. Horn, I. Mingareev and A. Werth: J.L.M.N.-Jour. Laser Micro/Nanoeng., 3, (2008) 114.
[15] I. Miyamoto, K. Cvecek and M. Schmidt: Phys. Procedia, 12, (2011) 381.
[16] S. Richter, S. Doring, F. Zimmermann, L. Lescieux, R. Eberhardt, S. Nolte and A. Tunnermann: Proc. SPIE, 8244, (2012) 824402.
[17] S. Richter, S. Doring, A. Tunnermann and S. Nolte: App. Phys. A, 103, (2011) 257.
[18] D. Hélie, M. Bégin, F. Lacroix and R. Vallée: App. Opt., 51, (2012) 2098.
[19] F. Lacroix, D. Hélie and R. Vallée: Proc. SPIE, 8126, (2011) 812612.
[20] P. Kongsuwan, G. Satoh and Y. L. Yao: Jour. Man. Sc. Eng., 134, (2012) 011004.
[21] W. Watanabe, S. Onda, T. Tamaki and K. Itoh: App. Phys. B, 87, (2007) 85.
[22] Y. Ozeki, T. Inoue, T. Tamaki, H. Yamaguchi, S. Onda, W. Watanabe, T. Sano, S. Nishiuchi, A. Hirose and K. Itoh: App. Phys. Expr., 1, (2008) 082601.
[23] A. Couairon and A. Mysyrowicz: Phys. Rep., 441, (2007) 47.
[24] S.L. Chin, S.A. Hosseini, W. Liu, Q. Luo, F. Théberge,N. Aközbek, A. Becker, V.P. Kandidov, O.G. Kosareva, and H. Schroeder: Can. J. Phys., 83, (2005) 863.

[25] K. Itoh and T. Tamaki: U.S. Patent 2010/0047589 (2010).
[26] R. B. Abernethy: ‘‘The New Weibull Handbook’’ ed. by R. B. Abernethy (R.B. Abernethy, Florida, 2000) p. 312.

(Received: May 29, 2012, Accepted: September 11, 2012)